Chitosan-Based Bilayer Hydroxyapatite Nanorod Composite Scaffolds for Osteochondral Regeneration

Shawn Swanson

A dissertation submitted in partial fulfillment of the requirements for the degree of

Master of Science in Materials Science and Engineering

University of Washington

2016

Committee:

Miqin Zhang

Peter Pauzauskie

Program Authorized to Offer Degree:

Materials Science and Engineering

University of Washington

Abstract

Chitosan-Based Bilayer Hydroxyapatite Nanorod Composite Scaffolds for Osteochondral Regeneration

Shawn Swanson

Miqin Zhang
Kyocera Professor
Materials Science and Engineering

Osteochondral defects involve injury to bone and cartilage. As articular cartilage is worn down, bone in the joint begins to rub together, causing bone spurs. This is known as osteoarthritis, and is a common issue among the aging population. This problem presents an interesting opportunity for tissue engineering. Tissue engineering is an approach to treatment of tissue defects where synthetic, three dimensional (3-D) scaffolds are implanted in a defect to facilitate healing. The osteochondral scaffold consists of two regions in the form of a bilayer scaffold- one to mimic bone with osteoconductive properties, and one to mimic cartilage with biomimetic properties. One approach to improving the osteoconductivity of tissue engineering scaffolds is the addition of hydroxyapatite (HAp), the main mineral phase in bone. HAp with nanorod morphology is desirable because it is biomimetic for the calcium phosphate found in bone. Incorporating HAp nanorods in bone tissue engineering scaffolds to form a composite material may increase scaffold osteoconductivity. The cartilage scaffold is fabricated from chitosan and hyaluronic acid (HA). HA is a known component of cartilage and thus is biomimetic. The bilayer scaffolds were seeded with osteoblast-like MG-63 cells to investigate cell migration and were evaluated with Alamar Blue proliferation assay. The cells successfully migrated to the bone region of the scaffold, indicating that the bilayer scaffold provides a promising osteochondral scaffold.

TABLE OF CONTENTS

LIST OF FIGURES

ACKNOWLEDGEMENTS

I would like to acknowledge Ariane for all of her hours dedicated to this project. I am frequently amazed at Ariane's knowledge of tissue engineering. She has become an expert in the field over the past few years, and has taken her time to teach me some of what she knows. I appreciate the time she gave from her chaotic schedule, and acknowledge that this project would not have been possible without her assistance. I would like to thank Professor Zhang for keeping me as a master's student and providing guidance, sitting through long phone calls, and always providing motivation. This has been a wonderful opportunity and I could not be more grateful that you took me in three years ago when I was an undergraduate. I will miss working with you and in the lab!

Chapter 1. INTRODUCTION

Osteochondral defects involve an injury to both bone and cartilage. Osteochondral tissue is located at the end of long bones, providing a transition from bone to articular cartilage for proper joint function. These defects are caused by degradation of articular cartilage by trauma or wear. Articular cartilage is the smooth cartilage on the end of bones that connects with joints and provides a smooth surface with a low coefficient of friction to allow for easy and proper joint movement. The articular cartilage tissue is free of blood vessels and nerves and only has one cell type: chondrocytes. Lacking vascularization, articular cartilage has a limited healing capacity. Subjected to severe biomechanical stresses, articular cartilage can be worn down, leading to osteoarthritis, which is the most common case of osteochondral defects[1]. When the articular cartilage tissue is worn down, the bone in the joint begins to rub together, causing pain and limiting proper joint function. Of the population over 65 years of age, 40% suffer from some form of osteoarthritis, decreasing quality of life in aging populations[2]. With the demographic changing as the number of people above the age of 65 increases, the need for a curative solution is increasing. Currently affecting 50 million adults in the US, by 2030 over 67 million adults are projected to be affected by osteoarthritis[3]. The most common clinical solution is a metal joint replacement, such as a total hip replacement (THR), requiring serious surgery with risk of infection. The mechanical stiffness disparity between the implant and the surrounding tissue leads to insufficient loading to the surrounding bone, causing more damage to the bone and eventual fibrous tissue encapsulation of the implant, limiting the life of a THR to 7-12 years[4]. Unfortunately, other solutions are not curative either- they only temporarily sedate the problem. Other treatment methods include autografts and allografts. Autografts are harvested directly from

the patient and then implanted to the affected area. This approach to treating defects is advantageous because an autograft contains the patient's cells and proteins that will promote healing. However, harvesting tissue from the patient creates another defect and surgical site that requires recovery. In addition, there is a limited supply of autograft from a given patient, limiting the size of the defect that can be repaired. Allografts originate from cadaveric bone and eliminate the possibility of morbidity associated with a second surgical site, but also decrease the success rate of the graft. To decrease the chance of disease transmission, allografts are disinfected, which eliminates the cells and proteins that help facilitate bone regeneration. The development of tissue engineering scaffolds can eliminate the need for palliative solutions, and instead provide a curative solution for the increasing aging population[5].

Tissue engineering is an approach to treatment of defects where synthetic, three-dimensional scaffolds are implanted in a defect to facilitate healing. A scaffold provides a structure to which surrounding native cells can adhere and proliferate in order to initiate the healing process. Theoretically, as the cells proliferate and organize to form new tissue, the scaffold begins to biodegrade into harmless by-products. A tissue engineering scaffold must be fabricated from a biocompatible and biodegradable material. Scaffolds should be porous, allowing for cell penetration, transport of nutrients and waste via diffusion, and neovascularization. Scaffold biocompatibility refers to the ability of the scaffold to elicit an appropriate response for the given application[6]. To be biocompatible a material must be non-antigenic and non-thrombogenic and interact with the host as desired. Desired interaction with the host can be pre-programmed into the biomaterial through surface material selection to support the intended function of the material, such as creating a hydrophilic surface for improved cell adhesion[7]. Biodegradation rates

of a scaffold should be quantifiable and tunable, as the scaffold material must degrade to allow for the formation of new tissue.

Combining both bone and cartilage tissue engineering yields a biphasic osteochondral scaffold. The osteochondral interface is an evolution of hard and soft bone to articular cartilage. The development of osteochondral tissue begins with the condensation of mesenchymal stem cells (MSCs) into aggregates under the effect of transforming growth factor (TGF-β). These aggregates allow for chondrocyte differentiation, which begin to secrete extracellular matrix (ECM), forming a cartilaginous precursor. Proliferation of the osteochondral progenitor cells also gives expression of SOX-9, a transcription factor that mediates the signaling of bone morphogenetic protein (BMP) during chondrogenesis and osteogenesis in the osteochondral region. Under influence of BMP and other growth factors, chondrocytes will organize into a structure called a growth plate at the osteochondral interface, from which bone will grow. The central part of this growth plate is the primary ossification center, where the collagen portion is replaced by bone, forming the osteochondral region[3].

Mimicking the osteochondral region has been done with gradient scaffolds. Gradient scaffolds have included tri-layers of collagen and hydroxyapatite with varying concentrations in each layer. This method included high concentrations of HAp of up to 70% in the bone region and 30% in the cartilage region, with corresponding collagen content. This scaffold was implanted in humans in a two year study and achieved partial defect regeneration, although tissue was inhomogeneous[8]. Additionally, this scaffold is expensive with the heavy collagen content. Porosity gradients in PCL scaffolds have also been studied for osteochondral defects applications, however, porosity gradients suffer from repeatability[9]. Our osteochondral scaffold is biphasic and fabricated from inexpensive materials, making it simple, repeatable, and cheap to

fabricate. To create a successful osteochondral defect scaffold, the cartilage and bone tissue engineering components of the scaffolds must be understood.

A successful cartilage tissue engineering scaffold for an osteochondral defect must be biomimetic to articular cartilage. Articular cartilage is composed of an extracellular matrix (ECM) with chondrocytes dispersed throughout the matrix. The ECM is composed of water, collagen, and proteoglycans[1]. Proteoglycans are proteins that form complexes with hyaluronic acid, collagen, and other matrix proteins in the ECM[10]. The connectivity of collagen and hyaluronic acid with the proteoglycans allows for the tissue to maintain its high water content, which is critical for maintaining the mechanical properties of the cartilage. Articular cartilage is made up of three zones- the superficial, middle, and the deep zone. The superficial zone makes up 10-20% of articular cartilage thickness and provides stress shielding for the rest of the cartilage. The high toughness of the superficial zone originates from the tightly packed and parallel orientation of collagen fibers to the direction of articulation, or the movement of the joint. This functions by providing a durable layer against the wear of compressive and shear forces of articulation. Chondrocytes in this region are flattened and dense, aligned with the orientation of the collagen fibers. The middle zone makes up 40-60% of the articular cartilage thickness and is composed of proteoglycans, a smaller amount of spherical chondrocytes, and obliquely organized collagen. While the superficial region provides resistance against fatigue from articulation, the deep zone provides compressive resistance with vertically aligned collagen and chondrocytes, making up 30% of the articular cartilage volume. The deep zone has less water and is denser than the other zones, transitioning to subchondral bone[1].

Current attempts for cartilage repair includes the autologous chondrocyte implantation (ACI) method. ACI is similar to an autograft- mature chondrocytes are harvested from an area of

the patient's damaged cartilage, and then the cell number is expanded in vitro. Once the cells have proliferated enough for treatment, they are implanted into the defect and sutured with a collagen membrane, isolating them in the defect. While the defect does indeed heal, histological results show that instead of regenerating articular cartilage, fibrocartilage is instead formed[11]. When cultured in vitro at high concentrations, chondrocytes produce Collagen 1, creating a fibrous and stiff tissue, which lacks the mechanical properties of the desired articular cartilage, and likely will be rejected by the body due to the mechanical mismatch. Mesenchymal stem cells (MSCs) have also been implanted in an articular cartilage defect with the same method as the ACI. Though allograft donor morbidity was eliminated, the same fibrous cartilage was formed[11; 12]. Cartilage tissue engineering can eliminate the need for the ACI method and help avoid implantation of fibrous cartilage. Popular scaffolds used for cartilage tissue engineering include collagen hydrogels, as collagen is a major component of articular cartilage. Due to high biocompatibility, collagen hydrogels showed high cell attachment and proliferation but lacked the mechanical integrity necessary for articular cartilage. Hyaluronic acid hydrogels were also used and had significant cell attachment, chondrocyte differentiation, and ECM production. However, this hydrogel also lacked the mechanical integrity that is necessary for the proper function of articular cartilage[11]. Instead, porous scaffolds are used in our bilayer system to provide higher mechanical stability, while maintaining high biocompatibility with the use of hyaluronic acid.

A successful bone tissue engineering scaffold should be osteoconductive to promote the differentiation of mesenchymal stem cells into osteoblasts, followed by collagen secretion to initiate bone formation. To increase the osteoconductivity of the scaffold, or the ability of the material to support osteoblast adhesion and proliferation, the scaffold should exhibit mechanical

strength similar to bone[13]. This similar mechanical strength increases the osteoconductivity of the scaffold because the mesenchymal stem cells test the elasticity of the matrix, which helps direct stem cell differentiation. Depending on the environment, mesenchymal stem cells can differentiate into several different cell types. The MSCs physically attach and pull on the matrix via their actin cytoskeleton, which experiences a resistance force that is proportional to the Young's modulus of the surface[14]. Having a similar stiffness to bone could help induce differentiation of MSCs into osteoblasts.

Current attempts of bone tissue engineering include Poly (lactic-co-glycolic) acid (PLGA) and bioactive ceramics. PLGA is a common material utilized for fabrication of bone tissue engineering scaffolds because it is biocompatible and biodegradable. Upon biodegradation PLGA releases lactic and glycolic acids. It also resists hydrolytic degradation and degrades in one to six months. However PLGA contributes to a decrease in local pH due to the release of lactic and glycolic acids during degradation, which leads to accelerated degradation of the polymer and inflammation of surrounding tissue. This sustained inflammation leads to the foreign body response, decreasing the functionality of the scaffold[15]. Bioactive ceramics such as calcium phosphate have been used for bone tissue engineering because they resemble the chemical composition of bone, increasing osteoconductivity and the scaffold's ability to bond with bone. However, the low biodegradation rates and the brittle nature of porous ceramics limits the potential for clinical use of bioactive ceramic scaffolds[16]. Instead, two naturally-derived polymers – chitosan and alginate – are used to fabricate the bone region of the biphasic osteochondral scaffold. A temperature-induced phase separation (TIPS) method is used to generate scaffolds with interconnected porosity. Chitosan, derived from crustaceans (crab and shrimp), is non-antigenic, non-toxic, cationic, biodegradable, and hydrophilic (promotes cell

adhesion), yet prone to swelling[13]. Alginate, derived from seaweed, is non-toxic and anionic, but proteins and cells cannot directly bind to its surface. Combining chitosan with alginate reduces the excessive swelling and weak mechanical properties associated with pure chitosan scaffolds as well as the lack of cell adhesion and protein adsorption (related to the surface chemistry of alginate) associated with pure alginate scaffolds. When the two polymers are combined, a polyelectrolyte complex forms due to the interactions between amine groups present in chitosan and carboxyl groups present in alginate. The mechanical strength and overall stability of chitosan-alginate polymer blend scaffolds is greater than that of pure chitosan or pure alginate scaffolds[13; 17]. A recent study conducted by our lab implanted chitosan-alginate (CA) scaffolds into critical-sized rat calvarial defects for in vivo evaluation of bone regeneration. CA scaffold implantation supplemented with cells and bone morphogenetic protein-2 (BMP-2) growth factor yielded the greatest defect closure of 71.56% over 16 weeks. This shows that the scaffold incited MSC differentiation into osteoblasts and osteoblast mineralization, and that the scaffold biodegraded with no adverse effect on bone formation[18].

The CA scaffold has been shown to be osteoconductive in the calvarial defect study, but if the osteoconductivity of the CA scaffold could be increased, the time for tissue regeneration could be reduced. One approach to improving the osteoconductivity of CA scaffolds is the addition of hydroxyapatite (HAp) to the polymer blend solution prior to scaffold fabrication. The chemical structure of HAp - $Ca_5(PO_4)_3OH$ – is similar to that of the mineral phase of bone[19]. The collagen in bone is organized in fibers, which are mineralized with HAp crystals[20]. Similarly, the CA scaffold acts as the matrix for the HAp, creating a reinforced composite much like the collagen-HAp network seen in bone. The HAp in bone has a nanorod morphology, so the use of HAp nanorods is desirable for tissue engineering because it is biomimetic. Nanorod morphology

allows attached cells to recognize morphology similar to their native matrix. HAp nanorods also provide a more bioactive morphology than traditional HAp platelets, as the nanorods have a larger surface to volume ratio, allowing for an increased release of calcium ions into solution- potentially inducing osteogenesis of surrounding bone cells. This suggests that incorporating HAp nanorods into CA scaffolds may increase the osteoconductivity of the CA scaffold.[5; 21].

Synthesis of HAp via classical methods yields micrometer-sized platelets[22]. Strict control of particle size and shape during nucleation requires more control than a simple precipitation process provides. Therefore, recent literature has demonstrated more precision in the precipitation process by controlling the solution pH, aging temperature, and time in an attempt to synthesize HAp nanorods. Optimization of these variables can result in precipitation of HAp nanorods[21; 22; 23]. Most popular synthesis methods use the hydrothermal process, which is not a biomimetic process. The hydrothermal process uses an autoclave to synthesize particles at high pressure and temperature[21]. It should be possible synthesize HAp nanorod with a biologically relevant method similar to how the body does- without the use of high pressure and temperature and harsh, inorganic surfactants.

To pursue a biomimetic synthesis of HAp nanorods, it is important to understand the process in vivo. HAp nanorod formation occurs inside an osteoblast. The process begins with elevated calcium ion concentrations in blood, which triggers BMP-2 production. The presence of BMP-2 incites a mesenchymal stem cell to pre-osteoblast transition. These pre-osteoblasts divide and secrete Collagen 1, which is the main fiber in bone. Alkaline phosphatase on the cell membrane begin to produce phosphate ions, and the pre-osteoblasts then mature into osteoblasts. Annexin channels on the osteoblast cell membrane transport calcium ions into the cell. At the same time, sodium and phosphate ions are pumped into the cell with the sodium ion pump. The

calcium and phosphate react, forming an amorphous calcium phosphate known as a HAp precursor. This precursor continues nucleation and growth in the high concentrations of calcium and phosphate ions inside the cell. The hydrogen atoms in the precursor are liberated, and pumped out of the cell with the sodium ion exchange pump, forming insoluble hydroxyapatite nanorods[24; 25].

In this work, a bilayer scaffold is used to mimic the osteochondral defect. Components for the bone and cartilage layers are optimized through biocompatibility screening of several scaffold types. Hyaluronic acid is implemented in the form of a tissue engineering scaffold in a complex with chitosan for the cartilage side of the scaffold. Hyaluronic acid is an anionic polymer, so when combined with chitosan, a cationic polymer, it forms a polyelectrolyte complex. The polyelectrolyte complex stabilizes hyaluronic acid, creating a mechanically stable scaffold with the combined bioactive and biomimetic properties of chitosan and hyaluronic acid[26]. Hyaluronic acid plays a large role in the formation of articular cartilage, making it a biomimetic inclusion to the cartilage tissue engineering scaffold. Chitosan and alginate scaffolds, previously shown to incite osteogenesis[18], are used in conjunction with hydroxyapatite nanorods. The addition of HAp nanorods should increase the osteoconductivity of the scaffold[17]. These two highly biomimetic scaffolds- chitosan/hyaluronic acid, chitosan/alginate with HAp combine to create a bilayer osteochondral scaffold to investigate the migration of cell types to the proper region. The concept behind the bilayer scaffold is that seeding both bone and cartilage cells onto the scaffold should result in cell migration to the proper region based on biological and mechanical cues. Thus if the scaffold was implanted in vivo, surrounding native cells would adhere to the scaffold and migrate to the proper region of the scaffold. Once the bone cells migrated to the bone region of the bilayer scaffold and the cartilage cells to the cartilage region of the scaffold, the

segregated cells would begin to proliferate. The cartilage cells would secrete ECM while the bone cells began to mineralize, regenerating the osteochondral defect.

Chapter 2. MATERIALS AND METHODS

2.1 MATERIALS

All chemicals were purchased from Sigma Aldrich and used as received unless otherwise noted. Hydroxyapatite nanorods were synthesized with sodium phosphate monobasic, calcium nitrate tetrahydrate, sodium citrate, 200 proof ethanol (Decon Labs), and 1M sodium hydroxide (EMD). Scaffolds were synthesized with practical grade chitosan from shrimp cells, hyaluronic acid sodium salt from *Streptococcus equi,* medium viscosity alginic acid sodium salt from brown algae, and glacial acetic acid (Macron). Scaffolds were processed with sodium bicarbonate (EMD), calcium chloride (J.T Baker), ammonium hydroxide solution (ACS reagent, 28-30% NH_3 basis). Cell culture was done with minimum essential medium (MEM, Gibco) and Dulbecco's modified eagle medium (DMEM, Gibco), which were supplemented with 10% fetal bovine serum (FBS, Gibco), and 1% antibiotic-antimycotic solution (AA, Gibco). TrypLE Express (Gibco), Dulbeccco's phosphate buffered saline (DPBS, Gibco), and agarose (SemKem) were also used for cell culture. All cell culture materials were sterile.

2.2 HYDROXYAPATITE NANOROD SYNTHESIS

A 0.75M sodium citrate solution was prepared by stirring 19.35 grams of sodium citrate into 100 mL of water. A 0.1M calcium nitrate solution was prepared by stirring 11.80 grams of calcium nitrate tetrahydrate into 233.3 mL of DI water and 166.6 mL of pure ethanol. The sodium citrate solution was added to the covered calcium nitrate solution using a peristaltic pump at 1.5 mL per minute using a magnetic stir bar. The pH of the resultant solution was brought to nine with dropwise addition of a 1M sodium hydroxide solution and stirred for 30

minutes. A 0.06M sodium hydrogen phosphate monobasic solution was prepared to achieve a calcium to phosphate ratio of 1.67 by stirring 3.60 grams into 333.3 mL of DI water and 166.6 mL of pure ethanol. The pH of the resultant solution was brought to nine with dropwise addition of 1M sodium hydroxide and stirred for 30 minutes. With both solutions on magnetic stir plates, the calcium nitrate solution was added to the sodium phosphate solution at 1.5 mL per minute with the peristaltic pump, displayed in Figure 1 below. 1M sodium hydroxide was added dropwise as needed to maintain a pH of nine. After addition was complete, the solution was heated to 37° Celsius on a hot plate and aged for two days with a magnetic stir bar. The pH was monitored for a few hours after heating and maintained at nine with occasional dropwise addition of 1M sodium hydroxide. The precipitate was filtered and washed with DI water three times, and dried in a drying oven overnight at 70° Celsius.

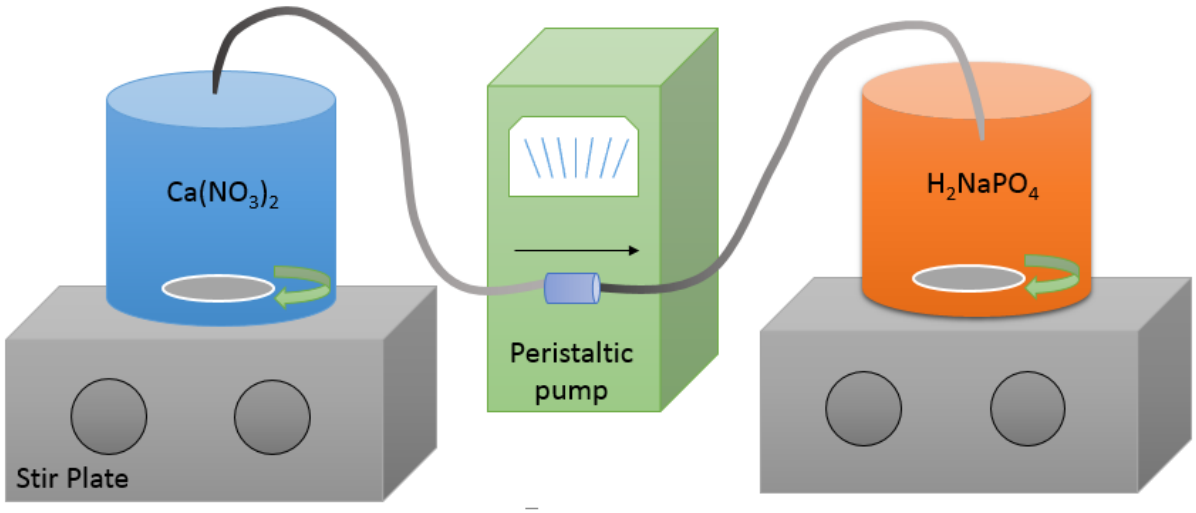

Figure 1: The experimental setup for nucleation of HAp using a peristaltic pump. Calcium nitrate and sodium citrate are added to sodium phosphate at 1.5 mL/min.

2.3 BILAYER SCAFFOLDS

2.3.1 *Experimental Approach*

Both layers of the osteochondral scaffold were optimized separately. Six different scaffold types were tested for the base material for the cartilage region of the osteochondral scaffold to investigate the base biocompatibility of the rat mesenchymal stem cells (rMSCs), which were derived from bone marrow. These scaffolds include 4% chitosan (C), 4% chitosan/hyaluronic acid (CHA), 4% chitosan/alginate (CA), 6% C, 6% CHA, and 6% CA. The scaffold that exhibited the highest proliferation over 14 days as shown through Alamar Blue was selected for the cartilage region of the osteochondral scaffold.

Four different scaffold types were tested for the base material for the bone region of the osteochondral scaffold to investigate the biocompatibility of the human osteoblast-like cells (MG-63s). MG-63s are cancerous osteoblasts, providing faster proliferation but with the same properties as the osteoblasts. These scaffolds include 4%C, 4%CA, 6%C, and 6%CA. The scaffold that exhibited the highest proliferation over 10 days as shown through the Alamar Blue proliferation assay was used in a panel to optimize the HAp concentration in the scaffold. Six concentrations of HAp were added to the optimized base scaffold, including 0.1%, 0.25%, 0.5%, 1%, 2%, and 3% HAp. The HAp concentration that yielded the highest proliferation over 14 days as shown through Alamar Blue was selected for the bone side of the osteochondral scaffold in conjunction with the optimized base material.

2.3.2 *Base Material Fabrication*

Batches of 4% C, 4% CHA, 4% CA, 6% C, 6% CHA, and 6% CA were synthesized for the optimization of the base material for the bone and cartilage region of the osteochondral

scaffold. 4% and 6% chitosan scaffolds were prepared similarly- four and six grams of practical grade chitosan were added to 99 and 98 mL of DI water with one and two grams of glacial acetic acid, respectively. The solutions were centrifuged three times each for three minutes at 2000 RPM and left overnight to soak. The samples were centrifuged once more for three minutes at 2000 RPM and then casted into 24 well plates. The casted solutions were then centrifuged for five minutes at 2000 RPM. The casted scaffold slurry was refrigerated overnight, placed in a -20° Celsius freezer overnight, and then lyophilized using a Labconaco freeze dryer. 4% CHA and 6% CHA were prepared similarly- the 4% and 6% chitosan solutions were prepared as outlined above, and two solutions of 1% hyaluronic acid (HA) were prepared. One gram of HA was added to 99 grams of water and one gram of glacial acetic acid. The solutions were centrifuged three times each for three minutes at 2000 RPM. The chitosan and hyaluronic acid solutions were left overnight to soak and then centrifuged once more for three minutes at 2000 RPM. The 4% and 6% chitosan solutions were added to a separate hyaluronic acid solution and centrifuged twice for five minutes at 2000 RPM. The mixed solutions were blended separately in a household blender for one minute and casted in a 24 well plate. The casted solutions were then centrifuged for five minutes at 2000 RPM. The casted scaffold slurry was refrigerated overnight, placed in a -20° Celsius freezer overnight, and then lyophilized using a Labconaco freeze dryer. 4%CA and 6%CA were prepared similarly. Four and six grams of alginate were added to 199 and 198 mL of DI water, respectively. The solutions were centrifuging three times each at 2000 RPM for three minutes. Once the alginate was dissolved, four and six grams of practical grade chitosan was added to the alginate solution and centrifuged once at 2000 RPM for three minutes and one and two grams of glacial acetic acid was added, respectively. The solutions were followed by immediate stirring and centrifuging two times at 2000 RPM for five minutes. The

solutions were then blended for five minutes in a household blender, placed in a cold water bath for 10 minutes, and then blended for five more minutes. The resultant slurries were casted in 24 well plates and centrifuged for five minutes at 2000 RPM. The scaffold slurry was refrigerated overnight, placed in a -20° Celsius freezer overnight, and then lyophilized using a Labconaco freeze dryer.

2.3.3 *CA/HAp Scaffold Fabrication*

A 6%CA solution was prepared as outlined above. After the 10 minute cold water bath, the 6%CA solution was split into six portions to prepare 0.1%, 0.25%, 0.5%, 1%, 2%, and 3% HAp concentrations. The HAp powder was ground with a mortar and pestle to break aggregates present from drying and then the proper amount was slowly added to the CA solution while stirring with a metal spatula. The solution was then blended for five minutes in a household blender, centrifuged once for three minutes at 2000 RPM, and casted in 24 well plates. The casted scaffolds were centrifuged once at 1000 RPM for five minutes. The well plates were refrigerated overnight, placed in a -20° Celsius freezer overnight, and then lyophilized using a Labconaco freeze dryer.

2.3.4 *Bilayer Scaffold Fabrication*

A 4% C and 1% HA solution were fabricated as outlined above. After the one minute blend, using a syringe, 1.5 mL of the prepared CHA solution was cast in each well of a 24 well plate and then centrifuged at 2000 RPM for five minutes. The covered well plate was then refrigerated for one hour. A 6%CA solution was prepared as outlined above. After the final blend, using a mortar and pestle to break up aggregates, one gram of hydroxyapatite powder was

slowly added to the solution while stirring, and then was blended for five more minutes. The CA/HAp was poured back into the centrifuge cup and centrifuged once at 2000 RPM for three minutes to eliminate bubbles from blending. After the casted CHA solution completed one hour of refrigeration, 1.5 mL of the CA/HAp solution was gently cast on top of the CHA solution. The casted bilayer scaffold was then centrifuged once at 1000 RPM for 5 minutes to connect the interface. The casted scaffold slurry was refrigerated overnight, placed in a -20° Celsius freezer overnight, and then lyophilized using a Labconaco freeze dryer. The fabrication schematic is shown in Figure 2 below.

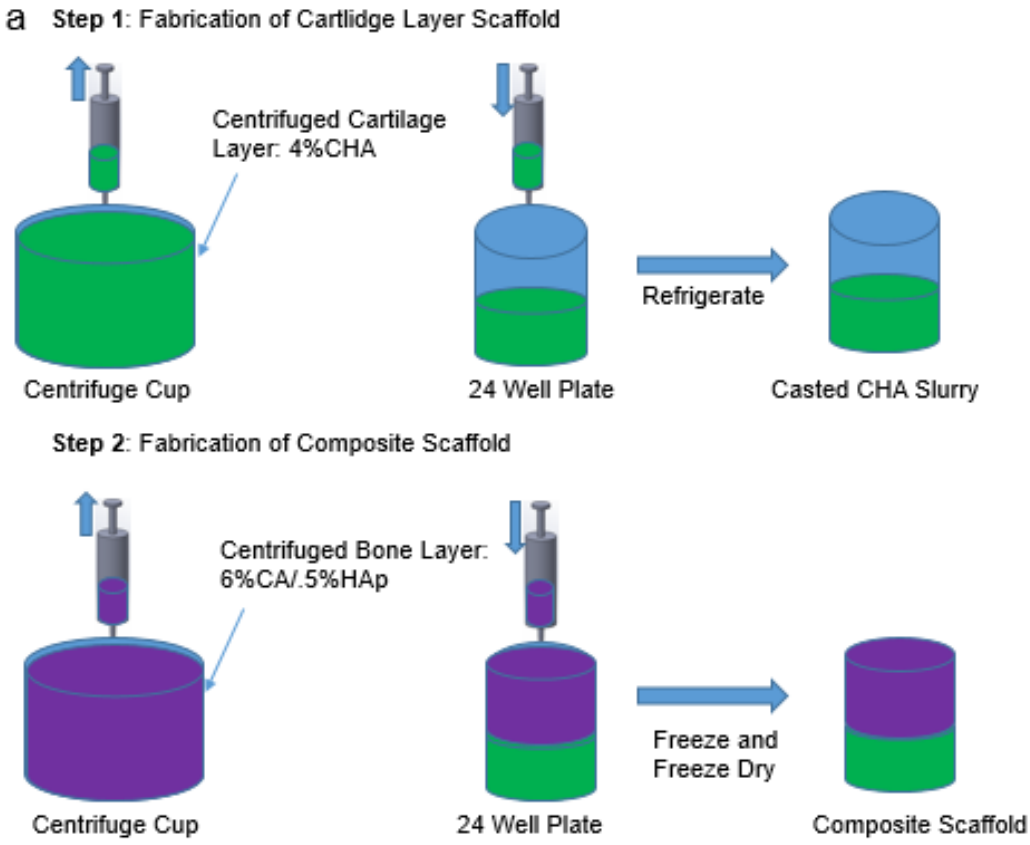

Figure 2: Schematic of bilayer scaffold fabrication. Step 1 shows the synthesis of the CHA layer, and Step 2 shows the addition of the CA/HAp layer.

2.3.5 *Scaffold Processing*

The scaffolds for the base material optimization were cut into 2mm thick disks and then quartered. Pure chitosan scaffolds were crosslinked by soaking the scaffolds in 1M sodium carbonate under a vacuum for one hour. CA and CA/HAp scaffolds were crosslinked with 0.2M calcium chloride and soaked under a vacuum for 15 minutes. CHA scaffolds were neutralized with 30% ammonium hydroxide for one hour under vacuum. The bilayer scaffolds were crosslinked/neutralized in a solution of 0.2M calcium chloride and 25% ammonium hydroxide for one hour under a vacuum. All of the crosslinked/neutralized scaffolds were rinsed with DI water three times, and left on a shaker at 60 RPM overnight. The scaffolds were sterilized by soaking in 70% ethanol under vacuum for one hour, with a solution change at 15 minutes. The ethanol was removed in a sterile hood and the scaffolds were rinsed 3X with sterile PBS, left in PBS overnight on a shaker at 60 RPM, and placed in sterile media one night before seeding.

2.3.6 *Scaffold Seeding*

Processed scaffolds were placed in 24 well plates, which were coated with 0.5 mL of a sterile 1% agarose solution. Pliers were soaked in 70% ethanol for 30 minutes and were used to move prepared scaffolds into the well plate. MG-63s were lifted with TripLE and counted with a hemocytometer. For the base material optimization, 20,000 cells (either MG-63s or rMSCs) were seeded in 10 microliters of media. For the bilayer scaffold, 200,000 cells were suspended in 10 microliters of media and seeded onto scaffolds with four methods, which are shown in Figure 3 below. Figure 3a shows seeding in the HAp side of the bilayer scaffold, and Figure 3b shows seeding on the CHA side of the bilayer scaffold. The scaffolds depicted in Figures 3c and 3d are

cut differently. Figure 3c shows seeding on top of the CHA region of the scaffold and Figure 3d shows seeding on top of the HAp region of the scaffold.

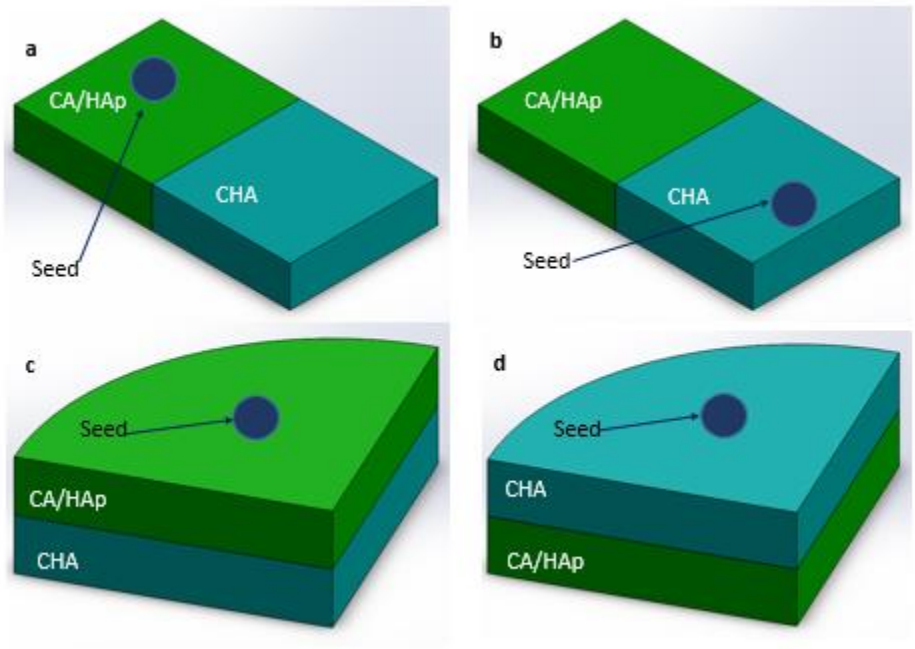

Figure 3: Seeding methods a) Cells seeded on the CA/HAp side of the bilayer scaffold b) Cells seeded on the CHA side of scaffold c) Cells seeded on top of the CHA region d) Cells seeded on top of the CA/HAp region.

2.3.7 *Scaffold Imaging*

Cells were dehydrated with dilutions of ethanol and then stained with DAPI (4',6-diamidino-2-phenylindole). The processed samples were imaged with optical microscopy and fluorescence imaging. The cells fluoresce blue and the scaffolds have an auto-fluorescence of green and red.

2.4 Cell Culture

Two cell lines were used, including rat mesenchymal stem cells (rMSCs) derived from bone marrow, and human osteoblast-like cells (MG-63s). RMSCs were cultured in Dulbecco's Modified Eagle's Medium (DMEM) supplemented with 10% FBS, and 1% AA at 37° C in a humidified incubator with 5% carbon dioxide. MG-63s were cultured in Dulbecco's minimum essential medium (MEM) supplemented with 10% FBS, and 1% AA at 37° C in a humidified incubator with 5% carbon dioxide. The media was changed every 2-3 days and split 4-5 times a month to avoid confluency.

2.5 Cell Proliferation Assay

Alamar Blue was used to track cell proliferation of the seeded scaffolds by following the protocol provided by Life Technologies. Briefly, a 10% solution of Alamar Blue was prepared by diluting the Alamar Blue stock solution 1:10 with the proper cell medium. Media was aspirated from the scaffolds and 1 mL of 10% Alamar Blue solution was added to each scaffold. The scaffolds were incubated for four hours at 37° C in a humidified incubator with 5% carbon dioxide. Four 200 microliter aliquots of Alamar Blue were transferred from the scaffolds to an opaque black 96-well plate. The fluorescence was measured on a SpectraMax M5 microplate reader (Molecular Devices) at excitation and emission wavelengths of 560 and 590 nanometers, respectively.

2.6 Fourier Transform Infrared Spectroscopy

The infrared spectra of the hydroxyapatite nanorods and the chitosan based scaffolds were characterized using a Thermo Scientific Nicolet 6700 FT-IR system using the KBr pellet method.

Briefly, scaffolds were frozen in liquid nitrogen and a mortar and pestle was used to create a fine powder. The powder was then diluted 1:10 with KBR, and pressed into a pellet. 270 scans of FTIR was ran with a KBR background.

2.7 Optical and Fluorescent Imaging

Optical and fluorescent images were captured with an Olympus optical microscope.

2.8 Scanning Electron Microscopy

Scanning Electron Microscopy samples were sputter coated with platinum and imaged with a JEOL JSM-7000F microscope.

2.9 Tunneling Election Microscopy

Samples for Tunneling Electron Microscopy were prepared with a copper grid using a Philips EM430 TEM.

2.10 Mechanical Testing

Compression testing was done with an Instron mechanical tester. Scaffold samples for the base material optimization were cut into two millimeter thick disks and crosslinked/neutralized. The bilayer scaffolds were taken from the well plate, and one mm was cut off from both sides of the scaffold. These cut scaffolds were then crosslinked/neutralized. All scaffolds were tested wet and were compressed 80% at a rate of 0.4 millimeters per minute.

2.11 X-Ray Dispersive Spectroscopy

X-Ray dispersive spectroscopy was done with Bruker F8 Powder XRD.

2.12 Porosity and Density Analysis

Porosity and density was measured by measuring the weight and dimensions of each scaffold, and then soaking in isopropanol under vacuum for 1 hour. The mass of the soaked scaffolds was then measured.

Chapter 3. RESULTS AND DISCUSSION

3.1 HAp Synthesis

3.1.1 *HAp Optimization*

Biomimetic pathways of HAp nanorod fabrication were investigated. This basic procedure allows for the screening of the pH, temperature, and aging time that HAp nanorods form. This was done by testing pH values of 7, 9, 10, and 11, temperatures of 37 and 70°C, and aging times of 18 hours, and 2, 4, and 7 days. Bulk hydroxyapatite powder was dissolved at pH 2 with dropwise addition of nitric acid. The supersaturated solution was precipitated with dropwise addition of 30% ammonium hydroxide to the desired pH and then aged for the proper time at the proper temperature. Figure 4 below depicts the experimental outline. This depicted procedure began with pH values of 7, 9, and 11, with pH values of 9 and 11 yielding nanorod structure. This pH range was focused on and further investigated with testing pH values of 9, 10 and 11, as outlined in Figure 4 below. Of these parameters of pH, temperature, and time, pH 9, aging 2 days at 37° C yielded the most attractive nanorods.

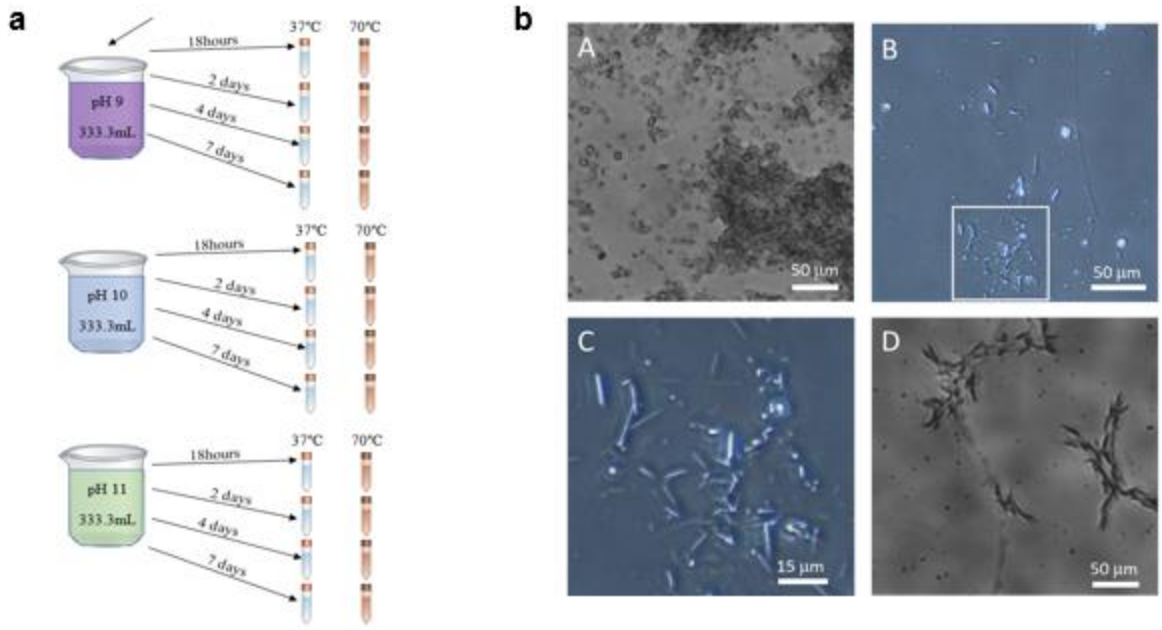

Figure 4: a) Temperature, pH and Aging Time Optimization Optical microscopy of representative HA samples. (B) a) 2 Days, 37ºC, pH 9 showing platelet structure b) 2 Days, 37ºC, pH 9 showing a mixture of platelet and nanorod structure c) Magnification of B showing nanorod structure with inconsistent particle size d) 2 Days, 37ºC, pH 9 showing optimized and consistent nanorod structure.

However, even the optimized pH, time, and temperature did not result in complete nanorod yield, there were also larger platelet morphology particles. Figure 4b shows the mixture of results. Though there was nanorod morphology (Figure 4b-d), it was mixed with platelet morphology (Figure 4a) and inconsistent particle sizes (Figure 4b-c). Filtering out the nanorods did not give a practical yield. The platelet morphology likely originated from HAp agglomeration during nucleation and growth. The HAp particles likely agglomerated because nanoparticles have large surface to volume ratios and thus have large surface energies, leading to attraction between particles. Common methods of avoiding nanoparticle agglomeration include

the use of surfactants. Surfactants stabilize single nanoparticles by surrounding the surface with like charges, inducing coulombic repulsion between particles, allowing for independent nucleation and growth[21].

The use of surfactants during synthesis is essential for achieving consistent particle size and morphology. Surfactants provide colloidal stability to a suspension of nanoparticles and can also guide the direction of nucleation and growth, tailoring the morphology. Affective surfactants can bond to the surface of the nanoparticle, so as to direct growth longitudinally and prevent aggregation. Since the surfactant bonds with the nanoparticle, it is desirable to have a biomimetic surfactant. Sodium citrate was used as a surfactant since it has excellent biocompatibility, bonds strongly with calcium ions, and even plays a role in bone growth in the body[21]. In a previous study where sodium citrate was used as a surfactant for HAp nanorod synthesis, the hydrothermal technique was used[21]. Pursuing a biologically relevant synthesis method, the hydrothermal technique was not used, and instead higher morphology control was achieved with the optimized pH, temperature, and aging time, as well as the addition of ethanol to the reaction system to provide further colloidal stability. The use of ethanol decreases the amount of water in the reaction system. Water, as a polar liquid, often induces particle agglomeration, so decreasing the water content of the reaction can increase the colloidal stability of the reaction[27]. Furthermore, sodium citrate is immiscible in ethanol, increasing the concentration of surfactant in the local miscible system, allowing for more thorough coating of the nanorods, further directing particle nucleation and growth[28]. The use of ethanol and the optimized parameters allows for the elimination of the autoclave during the reaction system.

The completed method, outlined in materials and methods, is biomimetic in several aspects. The synthesis occurs at 37° C, which is the temperature of in vivo HAp nanorod

synthesis. Additionally, the addition of sodium hydroxide mimics the sodium ion exchange pump. During in vivo HAp nanorod synthesis, the sodium ion channel pumps out hydrogen ions that were liberated during the hydrolyzation of the hydroxyapatite precursor and pumps in sodium ions. Adding sodium hydroxide to the system will eliminate hydrogen ions liberated from the precursor HAp as they combine with hydroxide ions, much like the cell pumping out the hydrogen ions. Similarly, the elimination of a hydrogen atom is accompanied by the addition of a sodium ion provided by the sodium hydroxide. The peristaltic pump allows for the slow addition of calcium ions to the phosphate solution to ensure that each nanoparticle is not chemically deficient and has plenty of surfactant to regulate growth. Immediately after the synthesized HAp solution was heated to 37°C, the pH began to drop below 9, indicating hydrolysis of precursor HAp. Although the majority of hydroxyapatite initially synthesized is pure HAp, the aging time allows for complete conversion of any precursor that may have been formed. Maintaining a pH of 9 with sodium hydroxide ensures complete conversion of precursor HAp to HAp nanorods. This method is novel in several ways. Previous methods that use sodium citrate as a surfactant use an autoclave to achieve nanorod formation[21]. This method instead uses biomimetic parameters and ethanol to further stabilize the system and nucleate HAp nanorods, making it a cheap and biologically relevant synthesis method.

3.1.2 *Characterization*

FTIR analysis was performed on a control HAp sample (Sigma Aldrich) and the synthesized HAp, shown in Figure 5 below. The control sample showed vibrational peaks characteristic of hydroxyapatite: OH^- at 3443 cm^{-1} and PO_4^{3-} at 1010 cm^{-1} and 565 cm^{-1}. This was compared to the synthesized sample, which closely resembles the control. The presence of

the OH- peak indicates that hydroxyapatite was formed[29]. XRD analysis yielded similar results. The characteristic peaks of hydroxyapatite are all present, which have been shown to indicate hexagonal HAp crystal structure, which is characteristic of hydroxyapatite[30]. These FTIR and XRD spectra are shown in Figure 5 below.

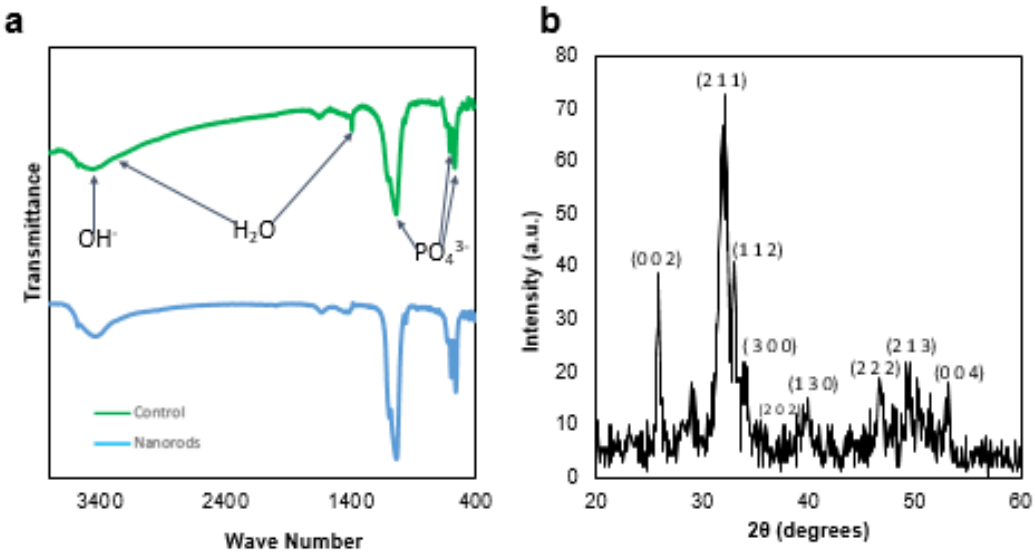

Figure 5: Chemical Analysis of HAp nanorods showing characterstic peaks of HAp a) FTIR b) XRD

3.1.3 *HAp Nanorod Morphology*

Morphological analysis was done with TEM, shown in Figure 6 below. TEM characterization revealed nanorod morphology. Particle sizes appear to fall between 100-200 nanometers in length.

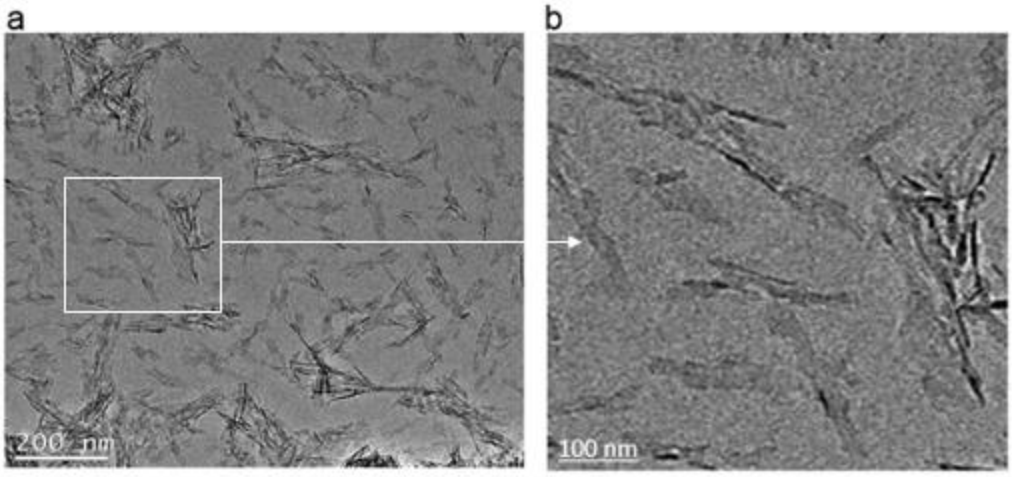

Figure 6: Morphology of HAp nanorods a) TEM b) Magnification of a showing nanorod strcuture.

Hydroxyapatite nanorods were successfully prepared with a biologically relevant synthesis method without the use of high pressure or temperature. This biomimetic synthesis route provides an alternative to the hydrothermal method- hydroxyapatite nanorods synthesis under low temperature and ambient pressure.

3.2 BILAYER SCAFFOLDS

3.2.1 *Cartilage Base Materials*

Alamar Blue proliferation assay was used to track the proliferation of rMSCs cells on the six base materials. RMSCs were used instead of MG-63s because these materials are for the cartilage region of the bilayer scaffold. Thus it is important to find the base biocompatibility of the scaffolds to a relevant cell line. RMSCs can differentiate into chondrocytes if given a biocompatible material. The largest proliferation of the rMSCs on a base material would indicate the most biocompatible material. Of the six scaffold types, 4%CHA and 6%CA supported the highest proliferation over a 14 day period, as shown in Figure 7 below. The highest proliferation

occurred on the 4%CHA scaffold. As mentioned before, hyaluronic acid plays a large role in the formation of articular cartilage[1]. Cells will recognize the chemical structure of HA, increasing the biocompatibility of the scaffold. The compressive modulus is nearly the lowest of all six scaffolds, which is desirable for imitating cartilage elasticity, shown in Figures 7b-c below. Though 4% C has the weakest mechanical strength, it had a much weaker fluorescence on Day 14, likely because it lacked the HA component that greatly increased the scaffold biocompatibility. SEM of the pore structure (Figures 7d-I) showed that scaffolds are interconnected and porous. Based on proliferation and mechanical strength, 4%CHA was chosen for the base material for the cartilage region of the scaffold.

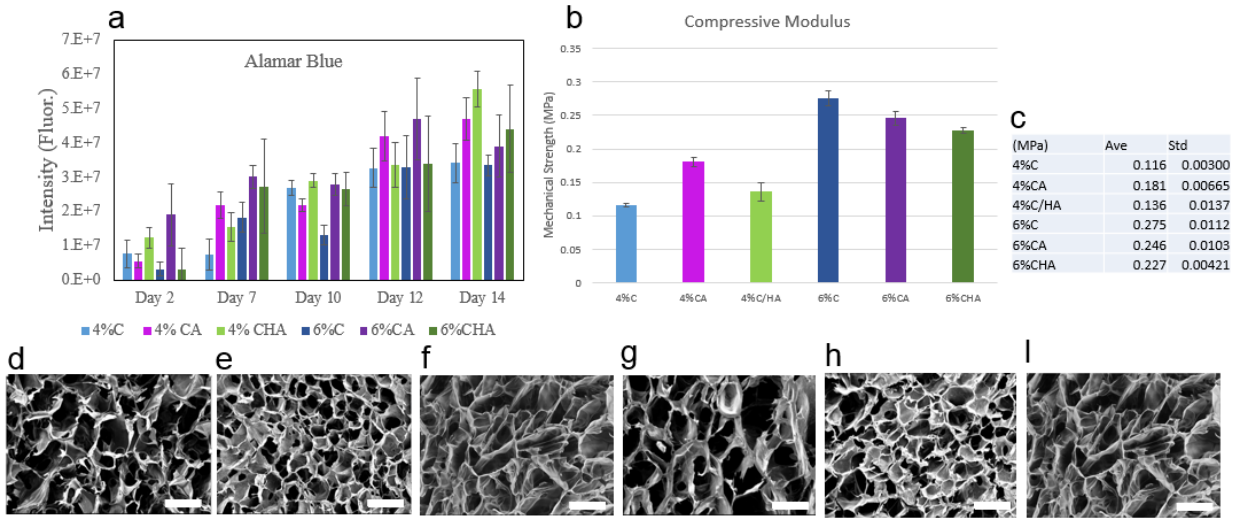

Figure 7: Cartilage base materials characterization. a) Alamar Blue showing proliferation of rMSCs on the base materials for Days 2, 7, 10, 12, and 14 b) Compressive modulus of the base materials in MPa c) Numerical values for compressive modulus in MPa. SEM panels of scaffold pores of the base materials. The scale bar is 200µm. d) 4%C e) 4%CA f) 4%CHA g) 6%C h) 6%CA I) 6%CHA

3.2.2 *Bone Base Materials*

Alamar Blue proliferation assay was used to track the proliferation of MG-63 cells on the four base materials. MG-63 proliferation on the four base materials was tracked in order to investigate the material which supported the highest MG-63 proliferation. Higher proliferation indicates better scaffold performance, allowing for the best material to be chosen. MG-63s were used because they are osteoblast-like cells, with faster proliferation due to their cancerous nature, allowing for faster base material optimization. These four materials were screened for biocompatibility before the addition of HAp so that a wider range of HAp concentrations could be tested, and to ensure that the material has a high biocompatibility even before the addition of HAp. The Alamar Blue assay was taken on Days 3, 5, 7, and 10. Of the four scaffold types, 6%CA supported the highest proliferation over a 10 day period, as shown in Figure 8a below. SEM images were taken of each base material to investigate pore structure and pore interconnectivity, shown in Figure 8d-g. All four scaffolds were seen to be porous and interconnected. Besides 6% C, 6%CA exhibits the highest compressive modulus of the four scaffold types. Since these scaffolds are the base material for a bone tissue engineering scaffold, a higher mechanical strength is desired so that it is closer to the stiffness of bone. As previously mentioned, cells pull on the matrix to test elasticity. The closer the elasticity of the synthesized matrix is to the elasticity of the cell's native matrix, the greater the biocompatibility[14]. Although 6% chitosan exhibited a larger compressive modulus than 6%CA, its fluorescence intensity was significantly less than 6%CA. Pure chitosan scaffolds suffer from swelling, which can decrease in vitro or in vivo mechanical properties, potentially decreasing biocompatibility of the scaffold. The addition of alginate to a chitosan scaffold forms a polyelectrolyte complex, increasing the stability of the scaffold and thus reducing swelling. 6% CA was chosen for the bone base

material due to its near comparable mechanical properties and larger fluorescence, indicating higher proliferation.

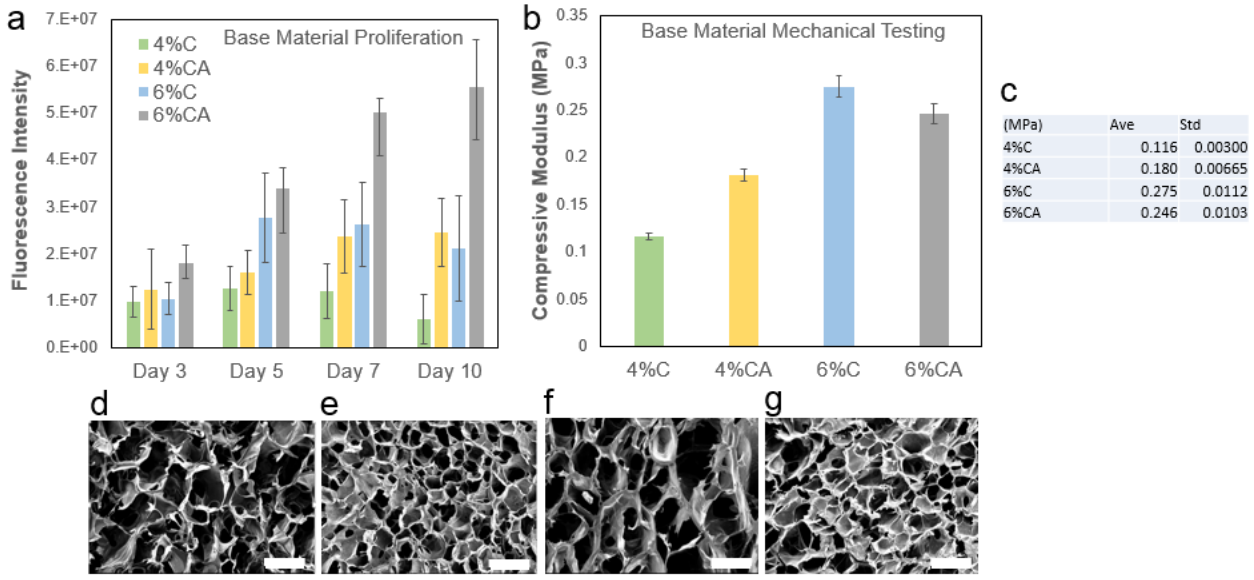

Figure 8: Optimization of the bone base material. a) Alamar Blue showing proliferation of MG-63s on the base materials for Days 3, 5, 7, and 10. b) Compressive modulus of the base materials in MPa and c) Numerical values for the compressive modulus values in MPa. SEM panels of the base materials. The scale bar is 200µm. d) 4%C e) 4%CA f) 6%C, and g) 6%CA

3.2.3 *Bone composite scaffolds*

A HAp panel was synthesized with 6% CA as the base material. HAp concentrations of 0.1%, 0.25%, 0.5%, 1%, 2%, and 3% were used. The assay was taken on Days 5, 7, 10, 12, and

14, shown in Figures 9a-b. Alamar Blue proliferation assay was used to track the proliferation of MG-63 cells on the six CA/HAp scaffolds.

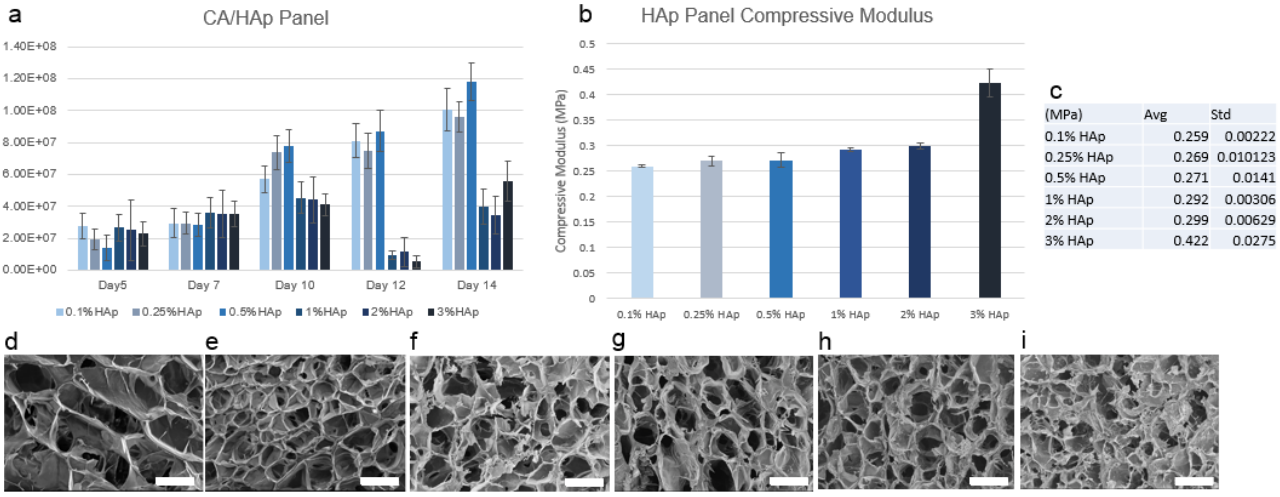

Figure 9: Optimization of HAp concentration in 6%CA scaffolds. a) Alamar Blue showing proliferation of MG-63s on the HAp panel and b) Compressive modulus of the HAp panel in MPa. c.) Numerical values for the compressive modulus values in MPa. SEM panels of scaffold pores of the HAp panel with increasing HAp. The scale bar is 200µm. d) 0.1 %HAp, e) 0.25% HAp, f) 0.5% HAp, g) 1% HAp, h) 2% HAp, and I) 3% HAp.

Of the six scaffold types, only 0.1%, 0.25%, 0.5% HAp gave positive proliferation. 1%, 2%, and 3% HAp began to lose structural integrity after Day 10, possibly because the high concentrations of HAp prevented complete crosslinking of the scaffold, causing it to slowly dissolve. Furthermore, Figures 9g-I show a limited porous network, possibly because the high concentration of HAp prevented the complete formation of the chitosan-alginate polyelectrolyte complex. The 0.5% HAp scaffold had the best proliferation of the three lower HAp concentrations, as seen in Figure 9a. This higher proliferation could be due to the larger HAp concentration among the mechanically stable scaffolds, making it a more biocompatible material. The 0.5% HAp scaffold had intermediate mechanical strength when compared to the panel-

however, it maintained structural integrity while 1, 2, and 3% HAp did not. Figures 9d-f show the pore structure of the HAp panel. Among the six scaffolds, the pore structure of 0.1, 0.25, and 0.5% (Figures 9d-f) look the most interconnected, while the other concentrations have limited interconnectivity. The 0.5% HAp concentration was used to form a 6%CA/0.5%HAp scaffold as the bone base material for the osteochondral scaffold.

3.3 Bilayer Osteochondral Scaffold

3.3.1 *Macroscopic imaging*

The bilayer osteochondral scaffold was fabricated with 6%CA/0.5%HAp for the bone region and 4%CHA for the cartilage region. The prepared scaffold slurries were subjected to mild centrifuging at 1000 RPM for five minutes after casting in 24 well plates in order to join the interface of the two materials. Macroscopic images in Figure 10 below displays the two regions with a seamless connection at the interface where use of an adhesive is unnecessary. Figure 10a is a cut and dry scaffold and Figure 10b is cut and crosslinked/neutralized scaffold.

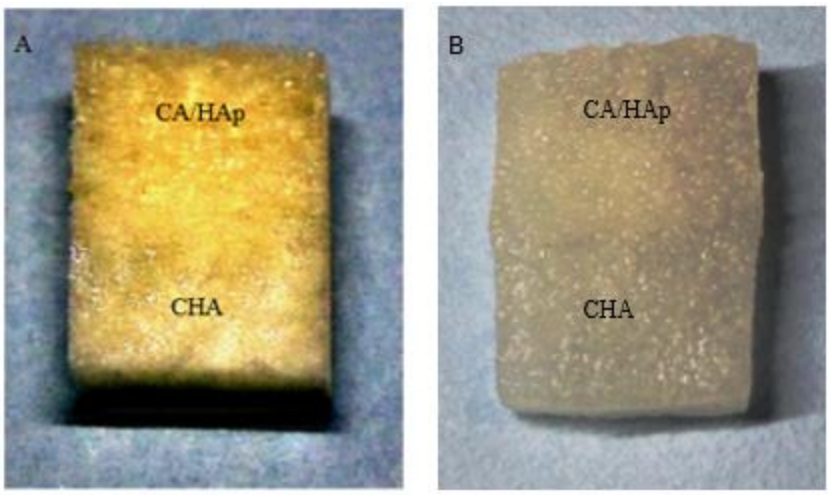

Figure 10: Macroscopic composite scaffolds a) Cut and dry bilayer scaffold b) Cut and wet bilayer scaffold

3.3.2 *Scanning Electron Microscopy*

The interface of the bone and cartilage regions was captured with SEM. The transition is well defined, and there seems to be a small mixing region of about 500 um, shown in Figure 11a below. This mixing region will provide a slight gradient for a smooth transition between the two regions as well as adding mechanical strength for proper integration of the two regions. Porosity and density analysis of the two sections indicate that 4% CHA is less dense with a higher porosity than 6%CA. These claims are supported by the significant difference in compressive modulus, shown in Figure 12 below. The higher porosity and lower density provides the smaller compressive modulus desired for a cartilage tissue engineering scaffold, while the opposite seen in the 6% CA provides the desired compressive modulus for a bone tissue engineering scaffold.

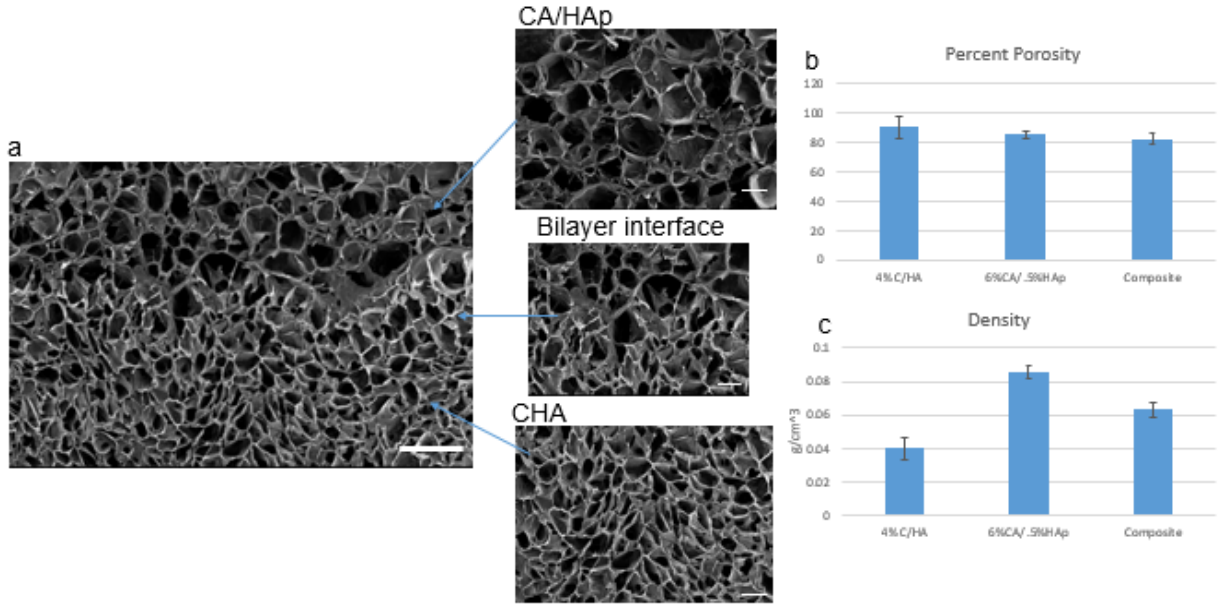

Figure 11a.) SEM panel of scaffold cross-section (scale bar is 500µm) + close up views of the CA/HAp, bilayer interface, and CHA (scale bar is 200µm) b.) Liquid displacement – porosity for the bilayer scaffold and its separate components c.) Density of the bilayer scaffold and its separate components.

3.3.3 *Mechanical Testing*

The bilayer scaffolds exhibited a bimodal curve- each section of the curve reflect stiffness values from the CA/HAp and CHA components. Figure 12 below shows curves of the bilayer scaffold and the two separated constituents.

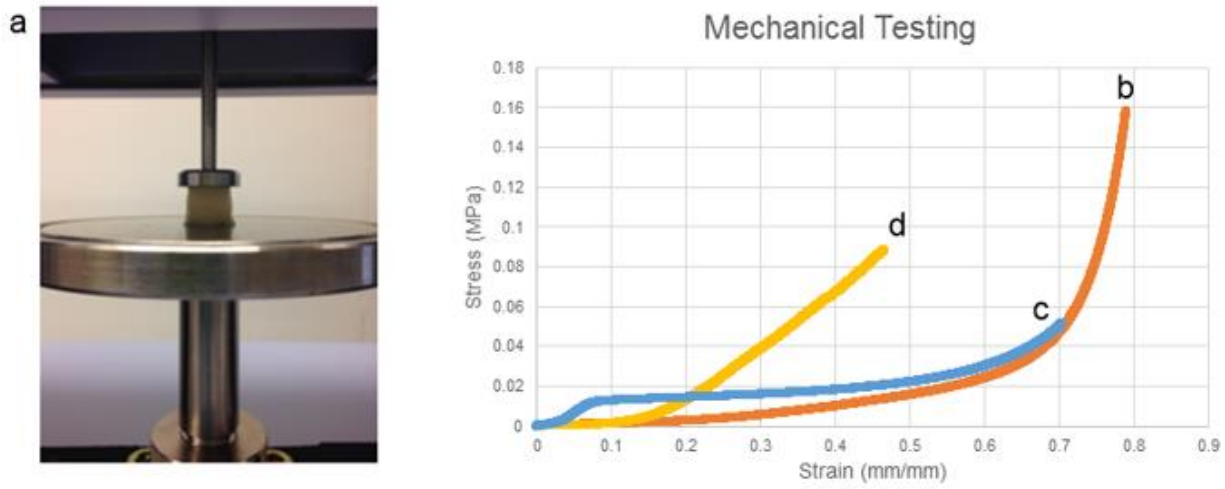

Figure 12: Mechanical testing curves. a) Compression testing setup of bilayer scaffold with CHA component on the bottom. b) Bimodal curve of bilayer scaffold which contains components of c and d. c) 4%CHA d) 6%CA/0.5%HAp

The bilayer scaffold exhibits CHA stiffness at strain values of 0.3-0.5 mm/mm, while it exhibits behavior of CA/HAp at strain values of 0.75-0.8 mm/mm. The bimodal curve (Figure 12b) shows a similar modulus to the separately tested CHA (Figure 12c) component but has a slightly larger CA/HAp modulus than that of the separate component (Figure 12d). This could be because the two regions of the bilayer added to each other during testing. The bilayers scaffolds were tested with CHA on the bottom, as shown in Figure 12a. As the less stiff component, this was compressed first. Once there was enough force to compress the CA/HAp, the CHA component was already significantly compressed. Comparing Figures 12c-d, the CHA scaffold is entering the densification region of a foam model of a stress strain curve around the same strain that CA/HAp scaffold begins to compress. This means that the compression of the CHA in the densification region likely contributed to the increase in the elastic modulus of the CA/HAp component of the bilayers scaffold when compared to pure CA/HAp.

3.4 Fourier Transform Infrared Spectroscopy

Chemical structure of the bilayer scaffolds were investigated with FTIR. The two regions were tested separately- with CHA and its components in Figure 13a and CA/HAp and its components in Figure 13b below.

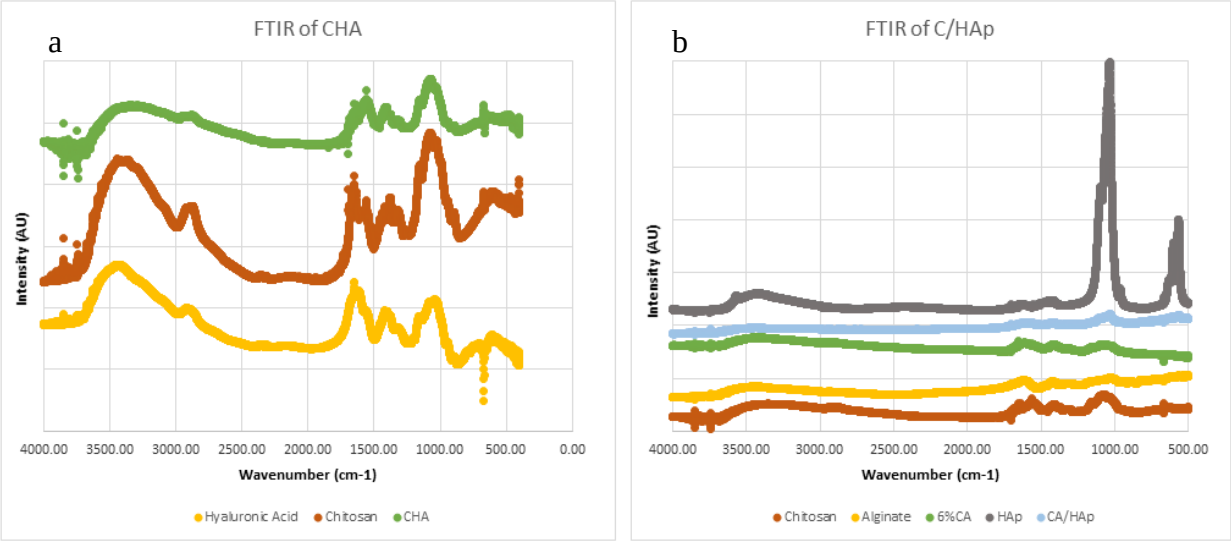

Figure 13a) FTIR spectra of CHA and components b) FTIR spectra of CA/HAp and its components.

Analysis of Figure 13a shows the characteristic peaks in chitosan and hyaluronic acid. The chitosan spectra shows its characteristic peaks at 1643 cm^{-1} for the amide-I, 1574 cm^{-1} for amide II, and 1173 cm^{-1} for the amino group[13]. The hyaluronic acid spectra shows its characteristic peaks at 1612 cm^{-1} for the carbonyl group, and similar amide I and II peaks to chitosan. The CHA peak shows a combination of peaks from its two constituents, with mild peak shifting from 1580 cm^{-1} to 1566 cm^{-1} indicating the formation of the polyelectrolyte complex. Peak ratios of the spectra are related to the polymer content of 4%CHA- chitosan is 4% of this scaffold while hyaluronic acid is only 1%, making the influence of chitosan on the CHA spectra more significant. The spectra suggests that the polyelectrolyte complex is formed with an ionic

interaction of the carboxyl groups of hyaluronic acid (COOH) and the amino groups of chitosan (NH_2)[26].

Analysis of Figure 13b shows the characteristic peaks of chitosan and alginate. The alginate spectra shows its characteristic peaks at 1620 cm^{-1}, and similar carboxyl and C-O stretching bands at 1424 and 1070 cm^{-1} to chitosan. The CA spectra have an intensified amide II peak, and near elimination of the amino peak, indicating the formation of a polyelectrolyte complex[13]. The phosphate peaks of the HAp spectra seem to only slightly affect the CA/HAp spectra, though the affect is limited due to the small concentration of HAp (0.5%).

3.5 Migration Study

Alamar Blue proliferation assay was used to track the proliferation on the seeded bilayer scaffolds using the first two seeding methods, the scaffolds that were seeded horizontally. Alamar Blue was taken on Days 3, 5, and 7 of the entire bilayer scaffolds. After Alamar Blue on Day 7, the scaffolds were cut in half along the interface of bilayer scaffold, trapping the cells on either side, and Alamar Blue was done on the separated components on Days 10, 12, and 14. Figure 14a below shows the proliferation of the two scaffolds on Days 3, 5, and 7, which were seeded on the CA/HAp side or the CHA side. Comparable cell proliferation is seen with both seeding methods.

Once these scaffolds were split in the middle of the bilayer, separating them into CA/HAp and CHA scaffolds, the cells were then stranded on either side of the scaffold. Figure 14b reveals the migration of the MG-63 cells to the CA/HAp side of the scaffold. Focusing on Day 10, the CHA scaffold that was originally seeded on the CHA side has approximately the same fluorescence as the other half: the CA/HAp scaffold.

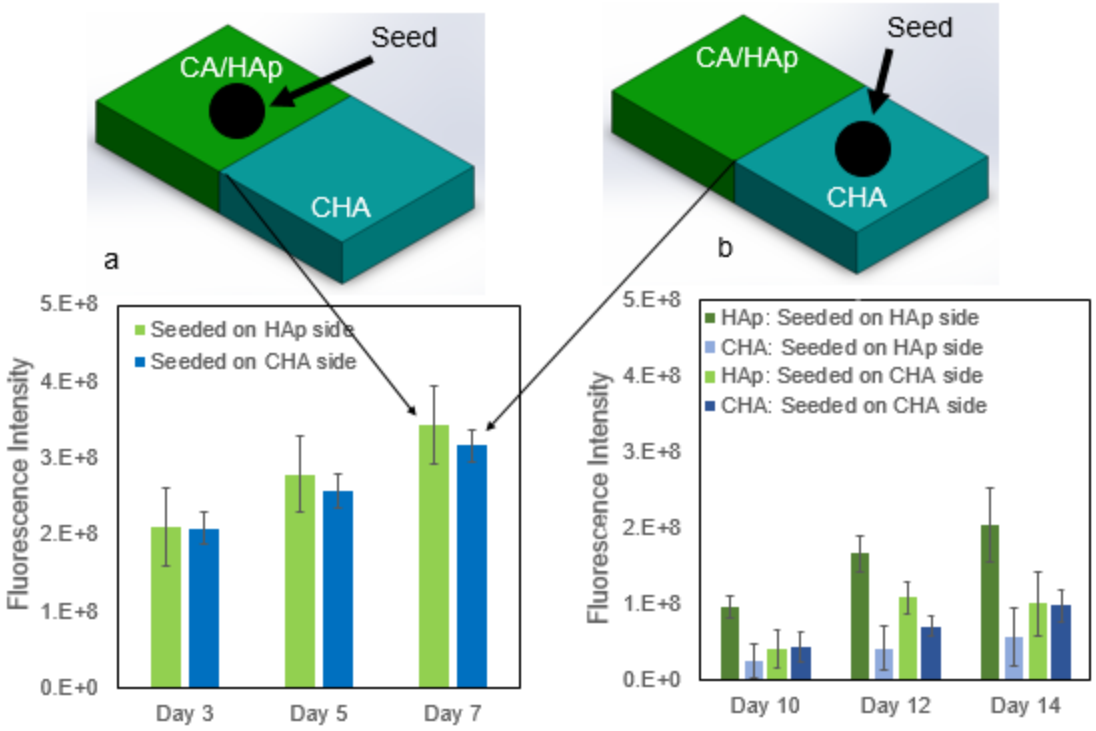

Figure 14: Proliferation of horizontal seeding methods on the bilayer scaffolds for a) Days 3, 5, and 7 and b) Days 10, 12, and 14 after cutting at interface.

This implies that the MG-63s migrated from the CHA side to the CA/HAp side of the scaffold, as this region originally had no cells. The small seeding volume of 10 µL ensured that the cells were focused completely on the CHA side of the scaffold. The HAp nanorods may have released calcium ions into the media, inciting MG-63 migration[31]. The increase of matrix elasticity could also attribute to the MG-63 migration, as the cells are actively pull on the matrix to test stiffness. Finding a stiffer matrix near the interface could cause the cells to migrate to the stiffer region, as this is similar to their native environment[14]. Furthermore, the HAp scaffold that was originally seeded on the HAp side has a fluorescence of nearly five times that of the respective CHA half. This indicates that the seeded MG-63s were generally content with staying and proliferating in the HAp region. The cells in both the HAp and CHA region continue to proliferate up to Day 14, with larger proliferation seen in the HAp side.

Fluorescence imaging supports the Alamar Blue data, as shown in Figure 15 below. All images were taken on Day 14. Images 15a-b show cell concentrations of the scaffold seeded on the CA/HAp side. Figure 15a in the CA/HAp region shows a dense concentration of cells (fluorescing blue), while Figure 15b in the CHA region shows a sparse concentration of cells. Cells seeded in the CA/HAp region of the scaffold generally did not migrate to the CHA region, as the CA/HAp region is more biocompatible. Figures 15 c-d show cell concentrations taken from the scaffold seeded on the CHA side. The images show a nearly equal concentrations of cells in both halves – agreeing with the Alamar Blue results which supported the idea that each region contained similar cell numbers. With the high cell activity in the CA/HAp region as shown with Alamar Blue (Figure 14b) and fluorescent imaging (Figure 15c), it is clear that the MG-63 cells migrated to the region of higher biocompatibility- possibly because of mechanical or biological cues provided by the CA/HAp scaffold.

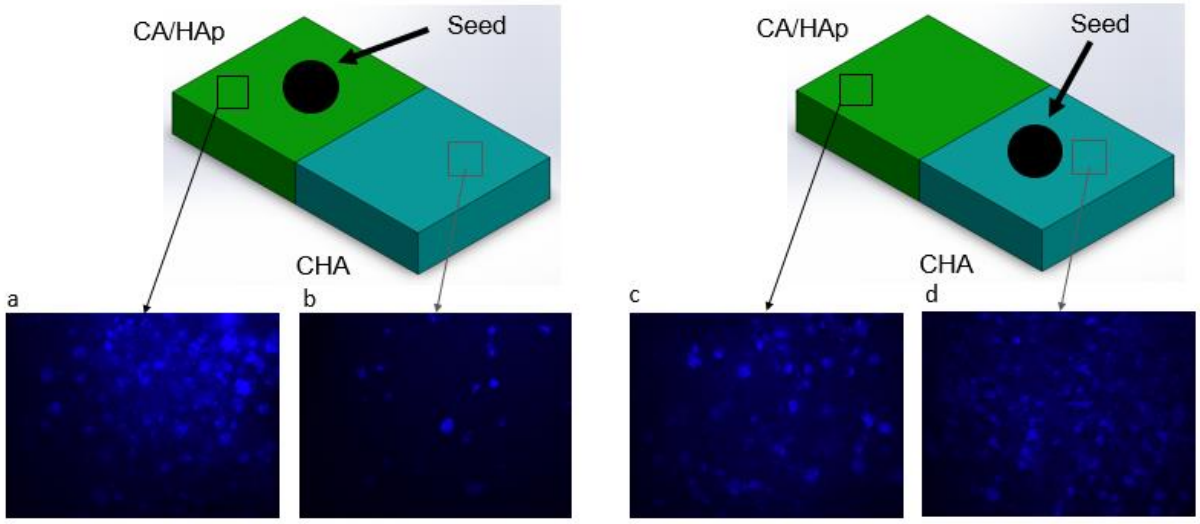

Figure 15: Images of cell concentrations on Day 14 using fluorescent microscopy a) CA/HAp scaffold, seeded on CA/HAp side b) CHA scaffold, seeded on CA/HAp side c) CA/HAp scaffold, seeded on CHA side d) CHA scaffold, seeded on CHA side

Alamar Blue of the vertically seeded scaffolds (seeding methods 3 and 4) are shown below in Figure 16, which shows proliferation over the 14 day incubation period. Cells were seeded on top of the HAp and CHA to investigate the ability of the cells to travel through the entire scaffold, as they were essentially seeded on either end of the bilayer.

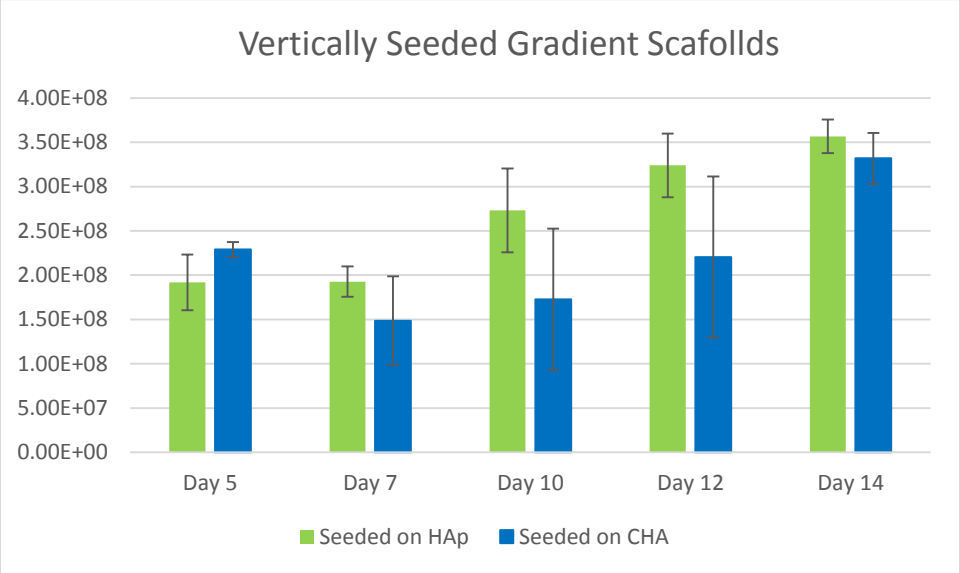

Figure 16: Alamar Blue of vertically seeded bilayer showing scaffold proliferation.

These scaffolds were not split in half but instead used for optical imaging to look at the concentrations of the cells in the two regions. Cell concentrations shown in Figure 17a-d below are visualized with cells fluorescing blue and the scaffold fluorescing green and red. Cells seeded in the CA/HAp region seemed to stay there. Figure 16a shows the CA/HAp region and reveals normal cell numbers, while Figure 16b shows that not many cells are visible in the CHA region.

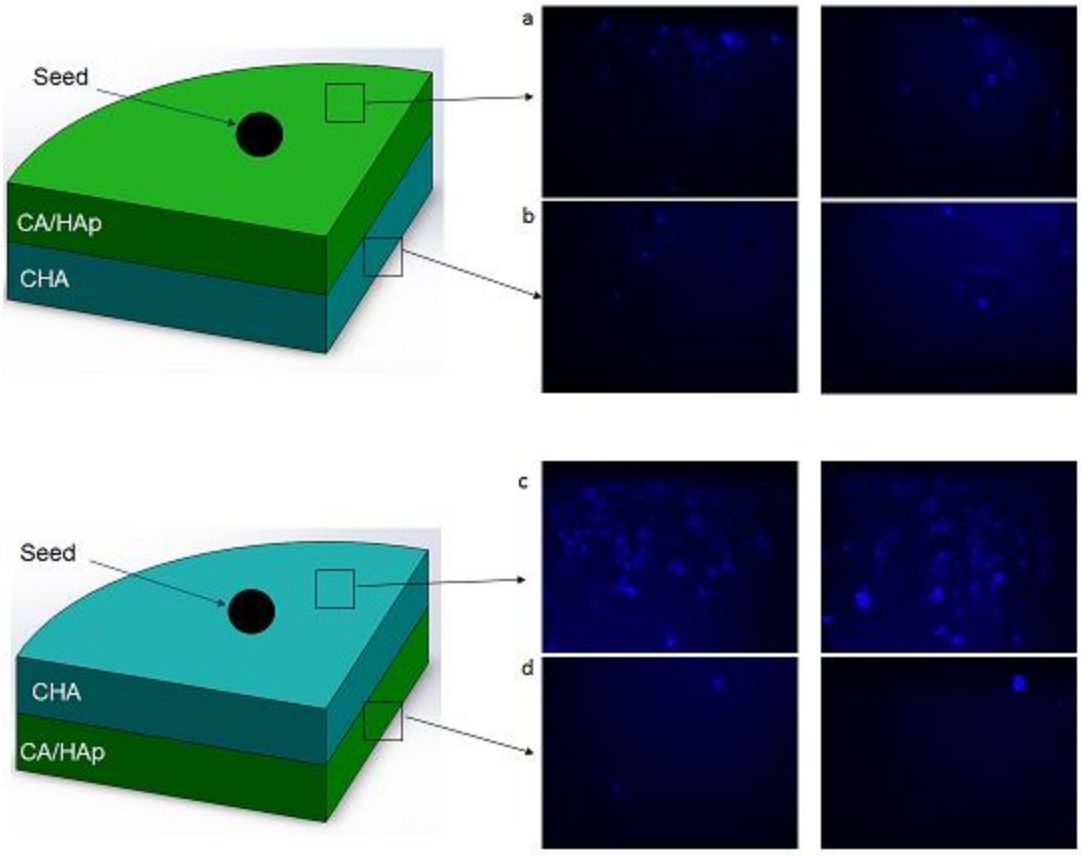

Figure 17: Fluorescence images of vertically seeded scaffolds showing cell concentrations a) CA/HAp, seeded on CA/HAp side b) CHA, seeded on CA/HAp side c) CHA, seeded on CHA side d) CA/HAp, seeded on CHA side.

Cells seeded on the CHA region showed a small amount of migration to the CA/HAp region. There are not many cells in the CA/HAp region (Figure 17d), which is possibly due to the long migration distance down the scaffold. Cells migrate slowly, and the migration distance in these scaffolds compared to the other two seeding methods is larger, inhibiting the number of cells that could reach the CA/HAp scaffold in 14 days.

Chapter 4. CONCLUSION

HAp nanorods were synthesized with a biomimetic method, eliminating the need for a high pressure and temperature synthesis seen in hydrothermal methods. A surfactant with an ethanol and water based reaction system created a stable colloidal suspension, allowing the HAp nanorods to nucleate under optimized pH, temperature, and aging conditions of pH 9, 37°C, for 2 days. Each material for the bilayer scaffold was separately optimized based on proliferation, mechanical testing, and pore structure. An optimized 6% CA/0.5%HAp and 4% CHA bilayer scaffold was fabricated through biocompatibility optimization of both layers. The HAp nanorod component increased the biocompatibility of the CA/HAp scaffold, as HAp nanorods are seen in bone. The HA component increased the biocompatibility of the CHA scaffold, as HA is a protein found in articular cartilage. The high biocompatibility of each region of the bilayer scaffold incited MG-63 migration to the bone region of the osteochondral scaffold, and MG-63s tended to stay in the bone region. MG-63 cells were successfully segregated, giving a promising potential for this scaffold for osteochondral defects. Future directions for the project include seeding both MG-63 cells and chondrocytes on the scaffold to investigate segregation of both cell types to the appropriate region of the scaffold. Successful in vitro cell segregation would suggest that when implanted in vivo, surrounding native cells will attach to the scaffold, and the bone and cartilage cells will migrate to the appropriate regions in the bilayer scaffold, resulting in proper cell segregation. With the successful segregation of MG-63s and the biocompatible cartilage region, it is likely that both cell types could be segregated.

BIBLIOGRAPHY

[1] FOX, A. S.; BEDI, A.; RODEO, S. A. **The Basic Science of Articular Cartilage Structure, Composition, and Function** Sports Health**:** 461-468 p. 2009.

[2] LUCA, A.; BLITTERSWIJK, C.; MORONI, L. **The osteochondral interface as a gradient tissue: From development to the fabrication of gradient scaffolds for regenerative medicine**: Birth Defects Research, Embryo Today: Reviews. 105**:** 34-52 p. 2016.

[3] KWON, K. et al. **Articular cartilage tissue engineering: the role of signaling molecules**: Cellular and Molecular Life Sciences. 73**:** 1173-1194 p. 2016.

[4] KRISHNA, V.; BOSE, S.; BANDYOPADHYAY, A. **Low stiffness porous Ti structures for load-bearing implants**: Acta Biomaterialia. 3**:** 997-1006 p. 2007.

[5] BAUER, T. W.; MUSCHLER, G. F. **Bone graft materials: an overview of the basic science**: *Clinical Orthopaedics and Related Research* 371**:** 10-27 p. 2000.

[6] RATNER, B. **The biocompatibility manifesto: biocompatibility for the Twenty-first century**. *Journal of Cardiovascular Translational Research* 28**:** 523-527 p. **2011**.

[7] OH, S. H.; LEE, J. H. **Hydrophilization of Synthetic Biodegradable Polymer Scaffolds for Improved Cell/Tissue Compatibility**: Journal of Biomedical Materials. 8 2013.

[8] FILARDO, G. et al. Treatment of Knee Osteochondritis Dissecans With a Cell-Free Biomimetic Osteochondral Scaffold Clinical and Imaging Evaluation at 2-Year Follow-up. **American Journal of Sports Medicine,** v. 41, n. 8, p. 1786-1793, Aug 2013.

[9] OH, S. H. et al. In vitro and in vivo characteristics of PCL scaffolds with pore size gradient fabricated by a centrifugation method. **Biomaterials,** v. 28, n. 9, p. 1664-1671, Mar 2007.

[10] YANAGISHITA, M. **Function of proteoglycans in the extracellular matrix.**: Acta Pathol Jpn. 43**:** 283-293 p. 1993.

[11] J.C., B.; G., V.-N. **Should we use cells, biomaterials, or tissue engineering for cartilage regeneration?**: Stem Cell Research & Therapy**:** 7-56 p. 2016.

[12] KOCK, L.; DONKELAAR, C. C.; ITO, K. **Tissue engineering of functional articular cartilage: the current status**: Cell Tissue and Research 347**:** 613-627 p.

[13] LI, Z. et al. **"Chitosan-alginate hybrid scaffolds for bone tissue engineering"** Biomaterials. 26**:** 3919-3928 p. 2005.

[14] ENGLER, A. J.; SEN, H. L.; SWEENY, D. E. **Matrix Elasticity Directs Stem Cell Lineage and Specification**: Cell. 126**:** 677-689 p. 2006.

[15] RAZAK, S. I.; SAIFUL, I. A.; SHARIF, N. F. **Biodegradable Polymers and Their Bone Applications: A Review.**: *International Journal of Basic & Applied Sciences* 12**:** 3131-43 p. 2012.

[16] RAMAY, H.; ZHANG, M. **Biphasic calcium phosphate nanocomposite porous scaffolds for load-bearing bone tissue engineering.**: Biomaterials**:** 5171-5180 p. 2004.

[17] LEVENGOOD, S. L.; ZHANG, M. **Chitosan-based scaffolds for bone tissue engineering**: Journal of Materials Chemistry B**:** 3161-3184 p. 2015.

[18] FLORCZYK, S. J.; LEUNG, M.; ZHANG, M. **Evaluation of three-dimensional porous chitosan–alginate scaffolds in rat calvarial defects for bone regeneration applications**: *Journal of Biomedical materials research* 100**:** 1974-83 p. 2012.

[19] FAIBISH, D.; OTT, S. M.; BOSKEY, A. L. **Mineral Changes in Osteoporosis A Review. Clinical orthopaedics and related research.**: C*linical Orthopaedics & Related Research* 448**:** 28-38 p. 2006.

[20] THIBAULT, R. A.; MIKOS, A. G.; KASPER, F. K. **Scaffold/Extracellular Matrix Hybrid Constructs for Bone Tissue Engineering.**: *Advanced healthcare materials*. 2**:** 13-24 p. 2013.

[21] JIN, X. et al. **Hydrothermal synthesis of hydroxyapatite nanorods in the presence of sodium citrate and its aqueous colloidal stability evaluation in neutral pH**: Journal of Colloidal and Interface Science. 443**:** 125-130 p. 2014.

[22] NAYAK, A. **Hydroxyapatite Synthesis Methodologies: An Overview**: International Journal of ChemTech Research. 2**:** 903-907 p. 2002.

[23] NATHANAEL, A. J. **Improved Mechanical Property of Hydrothermally Synthesized Hydroxyapatite Nanorods Reinforced with Polyethylene**: International Journal of Modern Physics. 24**:** 215-223 p. 2010.

[24] **Calcium & Phosphorus Metabolism**. R&D Systems' 2007 Catalog 2007.

[25] CLARKE, B. **Normal Bone Anatomy and Physiology**: Clinical Journal of the American Society of Nephrology. 3**:** 131-139 p. 2008.

[26] FLORCZYK , S. J. et al. **Porous chitosan-hyaluronic acid scaffolds as a mimic of glioblastoma microenvironment ECM**: Biomaterials. 38 2014.

[27] LUI, D. M.; TROCZYNSKI, T.; TSENG, W. J. **Water-based sol-gel synthesis of hydroxyapatite: process development.**: Biomaterials**:** 1721-1730 p. 2001.

[28] WANG, X. et al. **Liquid–Solid–Solution Synthesis of Biomedical Hydroxyapatite Nanorods**: Advanced Materials. 18 2006.

[29] BERZINA-CIMDINA, L.; BORODAJENKO, N. **Research of Calcium Phosphates Using Fourier Transform Infrared Spectroscopy**: Riga Technical University, Institute of General Chemical Engineering 2012.

[30] BRUNDAVANAM , R. K.; POINERN , G. E. J.; FAWCETT, D. **Modelling the Crystal Structure of a 30 nm Sized Particle based Hydroxyapatite Powder Synthesised under the Influence of Ultrasound Irradiation from X-ray powder Diffraction Data**: American Journal of Materials Science**:** 84-90 p. 2013.

[31] AYDIN, E.; PLANELL, J. A. **Hydroxyapatite nanorod-reinforced biodegradable poly(l -lactic acid) composites for bone plate applications**: Journal of Materials Science: Materials in Medicine**:** 2413-2427 p. 2011.